Environmental Science Nano

Exploring adsorption of neutral aromatic pollutants onto graphene nanomaterials via molecular dynamics simulations and theoretical linear solvation energy relationships

Journal:	*Environmental Science: Nano*
Manuscript ID	EN-ART-05-2018-000575.R1
Article Type:	Paper
Date Submitted by the Author:	19-Jul-2018

Complete List of Authors:	Wang, Ya; Dalian University of Technology, School of Environmental Science and Technology Comer, Jeffrey; Kansas State University, Anatomy and Physiology Chen, Zhongfang; University of Puerto Rico, Department of Chemistry Chen, Jingwen; Dalian University of Technology, School of Environmental Science and Technology Gumbart, James; Georgia Institute of Technology College of Sciences,

SCHOLARONE™
Manuscripts

Exploring adsorption of neutral aromatic pollutants onto graphene nanomaterials via molecular dynamics simulations and theoretical linear solvation energy relationships

Ya Wang,[abc] Jeffrey Comer,[*d] Zhongfang Chen,[c] Jingwen Chen,[*b] James C. Gumbart[*a]

[a] School of Physics, Georgia Institute of Technology, Atlanta, GA 30332, USA

[b] Key Laboratory of Industrial Ecology and Environmental Engineering (MOE), School of Environmental Science and Technology, Dalian University of Technology, Linggong Road 2, Dalian 116024, China

[c] Department of Chemistry, University of Puerto Rico, San Juan, PR 00931, USA

[d] Institute of Computational Comparative Medicine, Nanotechnology Innovation Center of Kansas State, Department of Anatomy and Physiology, Kansas State University, Manhattan, Kansas 66506-5802, USA

Abstract

Predicting adsorption of organic pollutants onto graphene nanomaterials is not only useful for exploring their potential adsorbent applications, but also helpful for better understanding their fate and risks in aquatic environments. Herein molecular dynamics (MD) simulations and theoretical linear solvation energy relationships (TLSERs) were employed to construct prediction models for adsorption of neutral organic pollutants onto graphene and graphene oxides. The MD simulations for adsorption of 43 aromatic compounds onto graphene and diverse models of graphene oxides with various functional groups (hydroxyl, epoxy and carbonyl) demonstrate that graphene has a stronger affinity for the aromatic compounds than graphene oxides. The hydroxyl and carbonyl groups of graphene oxides were found to form hydrogen bonds with the aromatic adsorbates, while epoxy groups did not. TLSER models were developed for predicting the adsorption equilibrium coefficients (K) onto graphene and graphene oxide nanosheets. In the graphene prediction model, H-donating ability (ε_α) and dispersion/hydrophobic interactions (V) have significant effects on log$K$ values, while in the graphene oxide model, ε_α is the most influential factor on log$K$ values. The models provide *in silico* approaches for predicting adsorption affinities onto graphenic nanomaterials.

Environmental significance

Graphene and its derivatives have an extraordinary propensity to accumulate adsorbed organic pollutants, which results in its potential applications as sorption materials in various fields. Meanwhile, the adsorption of organic pollutants on graphenic nanomaterials in aquatic environment can affect their environmental fate and brings potential ecotoxicological risks. Predicting the adsorption equilibrium coefficients and understanding the adsorption mechanisms towards graphenic nanomaterials is helpful for exploring the potential applications of graphene nanomaterials as well as evaluating their environmental risks. In this study, molecular dynamics (MD) simulations were carried out to systematically examine the adsorption behavior of 43 uncharged aromatic pollutants onto graphene and graphene oxides with different functional groups (hydroxyl, epoxy and carbonyl) at an atomic level. The results indicated that the interactions between neutral aromatic compounds and graphene are stronger than those between aromatic compounds and graphene oxides. Moreover, theoretical linear solvation energy relationships (TLSERs) models were first established for predicting the adsorption equilibrium coefficients on graphene and graphene oxides. These prediction models offer promising tools to obtain adsorption affinities onto graphenic materials.

1. Introduction

Owing to their unique physicochemical properties, graphene and its derivatives have drawn extensive interest since the discovery of graphene in 2004.[1,2] They have shown potential for applications in various fields, e.g., material science, medicine and biology, among others.[3-9] One interesting branch of these potential applications is the development of graphene-based sorption materials, which can be used for sample-preparation techniques, catalytic processes, wastewater treatment processes, etc.[10-12] On the other hand, graphene nanomaterials that are unavoidably released into the aquatic environment during their life cycle can also adsorb organic pollutants, thereby altering their environmental behavior, fate and toxicity.[13] Therefore, it is of great importance to investigate the adsorptions between organic pollutants and graphene nanomaterials, which is not only helpful for exploring their potential adsorbent applications, but also valuable for knowing more about their fate and risks in aquatic environment.

The adsorption of organic compounds on graphene oxide (GO), has also attracted increasing attention in recent years.[14-16] Like graphene, various interactions (i.e., van der Waals forces, hydrophobic interactions, electrostatic interactions, π-π stacking and hydrogen bonding interactions) may be involved in the adsorption processes onto graphene oxide.[17] The oxygen-containing functional groups, namely hydroxyl, epoxy, carbonyl and carboxyl, attached to the basal plane of GO can affect the interactions between organic compounds and GO. They can also change the hydrophobicity of graphene nanosheets, which affects the interactions between graphene nanosheets and water molecules.[18,19] For example, GO with moderate oxidation has the weakest adsorption capability for nitroaromatic chemicals among these adsorbents, viz., graphene, graphene oxide and reduced graphene oxide.[14] However, there is still a lack

of a systematic investigation about the influences of different functional groups attached to GO on the adsorption of diverse sets of organic compounds.

Recently, molecular dynamics (MD) simulations, which can provide an atomic-level view of adsorption, have been used for exploring the interactions between organic compounds and graphene nanomaterials.[20-23] Given numerous organic pollutants detected in the aquatic environment, it is not feasible to simulate the adsorption for compounds onto different graphene nanosheets one by one, even if MD simulation is more efficient than experimental determination. Thus, it is necessary to develop prediction models for estimating adsorption affinities of solutes on graphene and its derivatives.

In our previous study, we developed poly-parameter linear free energy relationships (pp-LFERs), which are based on Abraham descriptors, for predicting the adsorption energies of organic compounds onto pristine graphene in gaseous and aqueous phases.[24] However, these pp-LFERs are only applicable to the compounds having Abraham descriptor values, which are determined experimentally. Emerging pollutants lack these descriptor values, preventing the use of pp-LFERs. Theoretical linear solvation energy relationships (TLSERs),[25,26] on the other hand, can be developed using theoretical descriptors from molecular structures, overcoming the limitations of experimental data. Up to now, a TLSER prediction model for graphene has not been established, nor has a model for graphene oxide with different functional groups.

It is noteworthy that aromatic compounds, and particularly their halogenated derivatives, exhibit high affinities on the surfaces of graphenic materials,[27-30] and, coincidently, also constitute major pollutants of concern in natural waters and soils, including organochlorine pesticides [31] and brominated flame retardants. [32]

Considering that neutral chemicals generally show higher toxicity than their charged species,[33,34] which indicates that they may have higher environmental risk than the charged ones, in this study, we chose 43 uncharged aromatic organic compounds as adsorbate models. Additionally, different graphene oxides with functional groups (hydroxyl, epoxy and carbonyl) were built as adsorbent models. We systematically explored the adsorption mechanisms of 43 neutral organic compounds onto graphene oxides by MD simulations. Furthermore, we developed theoretical prediction models for the adsorption equilibrium coefficients onto graphene and graphene oxide nanosheets. These simulations provide insight into the adsorption mechanisms onto graphene oxides. Moreover, the prediction models developed in the current work can serve as an efficient, novel approach to obtain adsorption data for various uncharged compounds toward graphene and graphene oxides.

2. Computational details

2.1. Organic compounds and graphene nanosheet models

Herein, 43 neutral aromatic pollutants, including benzene and its derivatives (Table 1), were chosen as adsorbate models for their ubiquitous existence in natural waters and soils. Moreover, these 43 compounds have diverse functional groups, which is useful for probing the influence of functional groups on adsorption equilibrium coefficients. Their structures were downloaded from ChemSpider[35] and ChemicalBook.[36] These compounds were parameterized according to the CHARMM General Force Field (CGenFF),[37] using the ParamChem Web interface.[38,39]

A graphene sheet consisting of 160 carbons was built as an originally small periodic cell. In order to investigate the effects of functional groups attached to GO on adsorption, we built small periodic patches for graphene oxides sheets, i.e., graphene oxide with hydroxyl groups (GO_H), graphene oxide with epoxy groups (GO_E) and

graphene oxide with carbonyl groups (GO_C), having the same O/C ratio (0.125) which is comparable to the O/C ratio (0.12)[14] in the synthesized GO. The chemical compositions are $C_{32}(OH)_4$ for GO_H, $C_{32}O_4$ for GO_E and $C_{32}O_4$ for GO_C. We also built a periodic patch for graphene oxide with a mixture of hydroxyl and epoxy groups (GO_M), with a chemical composition of $C_{128}O_{12}(OH)_{24}$ and an O/C ratio (0.28), which is similar to the experimental O/C ratio (0.30).[14] The size for GO_M is three times larger than that for other graphene oxide models. Subsequently, these patches were solvated by adding water molecules, creating an ~30-Å layer of water between periodic images of the graphene sheet. To relax the structures for these graphene nanomaterials and verify their chemical stability, we simulated each solvated structure in a reactive molecular dynamics framework (ReaxFF).[40] For each structure, we performed energy minimization and 10 ps of equilibration at a temperature of 300 K and a pressure of 1 atm, using the ReaxFF implementation[41] of LAMMPS.[42] The parameters for the conventional molecular dynamics simulations were obtained by creating Kekulé representations (where aromatic bonds are represented by a consistent set of single and double bonds) of the structures produced by the ReaxFF energy minimization and submitting the results to the ParamChem web interface.[38,39] Thereafter, we tiled the periodic structures in the plane of the sheet, and built a 2 × 2 × 1 supercell for GS, a 5 × 5 × 1 supercell for GO_H, a 5 × 5 × 1 supercell for GO_E, a 5 × 5 × 1 supercell for GO_C and a 2 × 3 × 1 supercell for GO_M with the original small patches correspondingly, so that they have similar supercell sizes and are large enough to accurately accommodate adsorption of the solutes.

Subsequently, molecular dynamics simulations without imposing constraints on the supercells, were carried out using the software NAMD 2.12.[43] The final size of

the simulation cell for system including graphene and compounds was 39.1 Å × 42.3 Å × 39.3 Å. The sizes of supercells for systems including graphene oxides and chemicals were 49.3 Å × 42.6 Å × 41.6 Å (GO_H), 50.4 Å × 43.8 Å × 39.2 Å (GO_E), 48.9 Å × 43.2 Å × 41.0 Å (GO_C) and 40.2 Å × 51.9 Å × 40.4 Å (GO_M). The lateral dimensions of the supercells, i.e., those of the graphene plane, were free to fluctuate but did not change by more than 1 Å due to the periodicity of the graphene/graphene oxide layer. More details about adsorbent models are provided in Fig. 1.

Table 1. Organic Compounds and Logarithm Values of Calculated Adsorption Equilibrium Coefficients (log*K*) on Graphene and Graphene Oxides

No.	Compound	Substituents	log*K*_calculated				
			GS	GO_H	GO_E	GO_C	GO_M
1	benzene (PhH)		1.70	0.93	1.56	1.68	0.13
2	chlorobenzene (PhCl)	-Cl	2.92	1.56	2.49	2.54	0.82
3	bromobenzene (PhBr)	-Br	2.81	1.23	2.31	2.73	0.95
4	iodobenzene (PhI)	-I	3.26	1.56	2.49	2.84	0.79
5	phenol (PhOH)	-OH	2.65	1.37	2.04	2.33	0.89
6	benzonitrile (PhCN)	-CN	3.55	1.82	2.64	2.46	0.92
7	nitrobenzene (PhNO2)	$-NO_2$	3.99	2.16	2.66	2.62	1.90
8	toluene (PhMe)	$-CH_3$	2.67	1.10	1.97	2.13	0.21
9	phenylmethanol (PhMl)	$-CH_2OH$	2.52	1.76	2.10	2.09	0.93
10	ethylbenzene (PhEt)	$-CH_2CH_3$	2.73	1.49	2.30	2.55	0.87
11	propylbenzene (PhPr)	$-CH_2CH_2CH_3$	3.21	1.69	2.60	2.90	0.76
12	acetophenone (BzMe)	$-C(O)CH_3$	3.91	1.38	2.49	2.68	1.52
13	methylbenzoate (BzOMe)	$-C(O)OCH_3$	4.96	1.62	3.79	3.70	2.06
14	2-phenylethanol (PhEl)	$-CH_2CH_2OH$	2.97	1.47	2.53	2.67	1.04
15	phenylacetate (PhOAc)	$-OC(O)CH_3$	3.08	1.69	2.22	2.55	0.92
16	ethylbenzoate (BzOEt)	$-C(O)OCH_2CH_3$	5.45	1.97	3.68	3.93	2.30

17	4-fluorophenol (FPl)	-OH, -F	3.09	1.56	2.38	2.50	0.77
18	3-chlorophenol (ClPl)	-OH, -Cl	3.62	1.86	2.70	3.33	1.27
19	3-bromophenol (BrPl)	-OH, -Br	4.01	1.68	3.19	3.43	1.62
20	m-cresol (mCr)	-OH, $-CH_3$	3.30	1.50	3.06	3.01	1.18
21	p-cresol (PCRO)	$-CH_3$, -OH	3.63	1.41	2.85	3.21	1.42
22	4-ethylphenol (EPHE)	-OH, $-CH_2CH_3$	3.65	1.78	3.02	3.25	0.95
23	p-xylene (PXYL)	$-CH_3$	3.66	1.47	2.83	2.97	1.35
24	4-chlorotoluene (PCLT)	$-CH_3$, -Cl	3.58	1.70	3.18	3.09	1.61
25	4-nitrotoluene (NoT)	$-NO_2$, $-CH_3$	5.05	1.73	3.50	3.39	2.73
26	(3-methylphenyl) methanol (MeBl)	$-CH_3$, $-CH_2OH$	3.50	1.86	2.72	2.49	1.37
27	4-chloroanisole (ClAn)	-Cl, $-OCH_3$	4.19	2.32	2.95	3.04	1.95
28	4-chloroacetophenone (ClAh)	-Cl, $-C(O)CH_3$	4.79	1.99	3.48	3.18	2.05
29	1,3-dinitrobenzene (DNIN)	$-NO_2$	5.76	2.28	3.04	2.75	3.02
30	methyl 2-methyl benzoate (MMBa)	$-CH_3$, $-C(O)OCH_3$	5.13	1.52	3.84	3.64	2.22
31	4-chloroaniline (PhAm)	-Cl, $-NH_2$	3.12	1.60	2.32	2.72	1.50
32	3,5-dimethylphenol (dMPl)	-OH, $-CH_3$	4.50	1.14	3.65	3.23	2.13
33	hexabromobenzene (HBB)	-Br	9.52	1.82	5.85	4.68	4.24
34	pentabromotoluene (PBT)	-Br, $-CH_3$	9.55	1.95	6.37	4.62	4.92
35	1,2-dibromo-4-(1,2-dibromoethyl)-cyclohexane (TBE)	-Br, $-CHBrCH_2Br$	5.87	2.66	3.95	3.68	2.05
36	tetrabromo-*o*-chlorotoluene (TBCT)	-Cl, -Br, $-CH_3$	9.08	1.96	5.85	4.10	5.05
37	naphthalene (NAFT)		4.26	1.33	4.14	4.20	2.22
38	biphenyl (PhPh)		5.09	2.11	4.67	4.68	2.71
39	1-methylnaphthalene (MeNh)	$-CH_3$	5.21	1.73	4.92	4.41	2.60
40	BDE209 (B209)	-O-, -Br	9.65	2.32	5.85	5.27	2.59
41	BDE47 (B47)	-O-, -Br	5.85	3.83	4.13	4.41	2.63
42	BDE99 (B99)	-O-, -Br	6.06	3.92	5.00	5.21	4.22

43	BDE207 (B207)	-O-, -Br	9.39	4.06	5.63	4.28	5.12

GS: graphene sheet; GO_H: graphene oxide with hydroxyl groups; GO_E: graphene oxide with epoxy groups; GO_C: graphene oxide with carbonyl groups; GO_M: graphene oxide with mixed hydroxyl and epoxy groups.

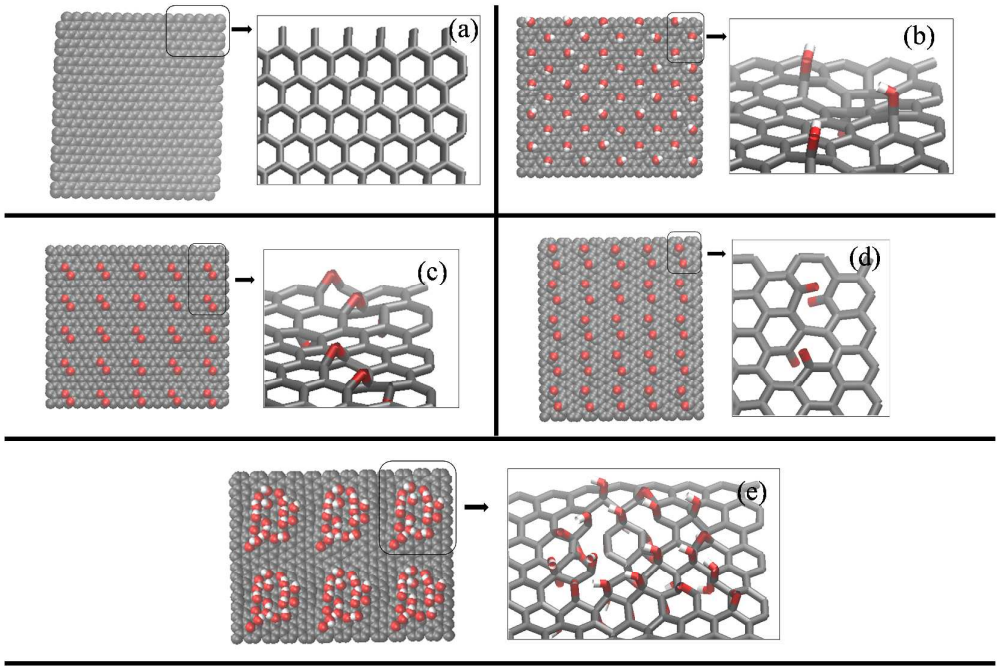

Fig. 1 The structures for graphene and graphene oxides. (a) graphene (GS); (b) graphene oxide with hydroxyl groups (GO_H); (c) graphene oxide with epoxy groups (GO_E); (d) graphene oxide with carbonyl groups (GO_C); (e) graphene oxide with a mix of hydroxyl and epoxy groups (GO_M).

2.2. Parameterization of graphene nanosheets

Note that these graphene and graphene oxides models were not directly parameterized according to CGenFF; although simulations representing graphene by the standard aromatic carbon type of CGenFF (namely CG2R61) yielded excellent correlation with experiments, our previous studies found that the adsorption equilibrium constants were underestimated by a factor of about 8.[28] To improve

agreement with the equilibrium constants, we made modifications to the specific Lennard-Jones size parameter (called NBFIX in the CHARMM framework) between sp^2 graphenic carbon atoms and water oxygen atoms. The parameter σ (C_{graph} and O_{water}) was shifted from its original value (0.1031843 kcal/mol) by $j\Delta\sigma$, where j was an integer $-8 \leqslant j \leqslant 8$ and $\Delta\sigma = 0.005$, producing 16 force field variants. The logarithms of the adsorption equilibrium constants (log$K$) were calculated for four compounds (BzOMe, PhEt, NoT, and PrBn) for each force field variant as described by Comer *et al*.[28] Here, "log" denotes a base-10 logarithm and K has units of mL/g. The variants with $j = -2$ and -3 gave mean log$K$ values for the four compounds in the closest agreement with experiment; thus, the calculations for these two variants were extended to 29 aromatic compounds with various physicochemical properties,[28,44] for which experimental log$K$ values were available and in a range of 1.96 ~ 5.68. The variant $j = -3$ yielded the best agreement with experiment, having a mean log$K$ of 3.69 over all 29 compounds, similar to the mean of the experimental values, 3.66. In addition to the reduced mean deviation from experiment in comparison to the standard CGenFF parameters, this force field variant also yielded improved correlation with experiment: $r = 0.920$. Hence, all simulations were performed with σ (C_{graph} and O_{water}) = 0.0881843 kcal/mol. Since this special Lennard-Jones parameter was parameterized to represent graphene-like carbon, it applied only to sp^2 carbon atoms in the graphene oxide structures (sp^3 atoms retained standard parameters).

2.3. Molecular dynamics simulations

All the molecular dynamics simulations for the systems including graphene nanomaterials and each aromatic compound were performed with NAMD 2.12. The TIP3P water model,[45] an all-atom explicit-solvent model typically used with the CHARMM force field, was used for simulating the aqueous environment. The

temperature and pressure were set 300 K and 1 atm, by using Langevin thermostat and Langevin piston methods,[46] respectively. A timestep of 2 fs was set for bonded interactions and short-range non-bonded interactions. The cut-off was set at 9 Å; the particle-mesh Ewald algorithm[47] was employed to treat the long-range electrostatic interactions every other time step. Analyses were performed with VMD 1.9.3.[48]

2.4. Calculation of adsorption equilibrium coefficients (*K*)

Every system underwent 1000 steps of energy minimization and 0.5 ns of equilibration before the calculation of free energies, which were obtained with the adaptive biasing force (ABF)[49,50] method. The Colvars module[51] of NAMD 2.12 was used to implement ABF along the z component of the vector between the center of mass for the organic compounds and the center of mass for the graphene or graphene oxide nanosheets. All the calculations were performed using a window with an interval $3 \leq z \leq 15$ Å, and the forces were sampled in bins with a width of 0.05 Å. Each simulation was run for 50 ns. To verify convergence of the free energy, a few systems were run for an additional 50 ns and no significant change was observed. The potentials of mean force from the 50-ns simulations were normalized so that the mean value on $14< z < 15$ Å was zero.

The adsorption equilibrium coefficients can be estimated with the method defined by Comer *et al.*:[28]

$$K^{\mathrm{calc}} = \frac{\sigma}{M}\int_0^{\mathrm{c}} \mathrm{d}z\, \mathrm{e}^{-\beta W^{\mathrm{calc}}(z)} \quad (1)$$

where $\beta = (k_{\mathrm{B}}T)^{-1}$ represents the reciprocal thermal energy, and $W^{\mathrm{calc}}(z)$ is the potential of mean force calculated by ABF. σ/M denotes the specific surface areas of the graphene nanomaterials. Here, the experimentally measured K values by the Brunauer-Emmett-Teller method,[14] 298.8 m^2/g for GS, GO_H, GO_E and GO_C, and 7.707 m^2/g for GO_M, are used to compare with our simulation results.

2.5. Theoretical descriptors for prediction models

All the molecules were optimized at the M06-2X/6-31G(d, p)[52] level using the GAUSSIAN 09 program unless stated otherwise.[53] The LANL2DZ basis set[54] was used for Br and I atoms. All the optimized structures were confirmed to be local minima by vibrational frequency analyses. Quantum chemical descriptors, including molecular polarizability, atomic charges, the highest occupied molecular orbital energy level (E_{HOMO}) and the lowest unoccupied molecular orbital energy level (E_{LUMO}) values, were extracted from the Gaussian output files. McGowan volumes were generated by using Dragon software[55] with the optimized structures. According to theoretical linear solvation energy relationships,[56,57] we used six theoretical descriptors for developing prediction models, which can be expressed as follows:

$$\log K = a\varepsilon_\alpha + b\varepsilon_\beta + fq^+ + eq^- + vV + p\pi + g \quad (2)$$

where log$K$ represents logarithm of the experimentally determined adsorption equilibrium constant; ε_α ($E_{LUMO} - E_{HOMO(water)}$), in an energy unit of electron volt (eV), is defined as covalent acidity; ε_β ($E_{LUMO(water)} - E_{HOMO}$) in eV, is covalent basicity; q^+, the most positive formal charge on a hydrogen atom in the molecule in atomic charge unit (acu), is taken as electrostatic acidity; likewise, q^- (acu), the absolute value of the most negative formal charge in the molecule, represents the electrostatic basicity; V is obtained by dividing the molecular volume (V_x, in mL/mol) by 100; π, a unitless quantity, is calculated by dividing the polarizability by V. a, b, f, e, v and p are fitting coefficients, and g is a regression constant. $a\varepsilon_\alpha$, $b\varepsilon_\beta$, eq^- and fq^+ describe the hydrogen bonding terms; vV characterizes bulk/cavity term; and $p\pi$ is the dipolarity/polarizability term. By convention, the logarithm in equation (2) is base-10 and the K has units of mL/g.

2.6. Models development and characterization

The calculated log*K* values for 43 organic compounds were used for establishing and validating models. We randomly split the 43 organic compounds into a training set of 35 aromatic compounds and a validation set of 8 aromatic compounds with a ratio of 4:1 (Table S1 of the Supplementary Information, SI). These parameters, namely, the determination coefficient (R^2), root mean square error (*RMSE*), Q^2 from bootstrap resampling (Q^2_{BOOT}) (1/5, 5000 iterations) and external explained variance Q^2_V were used to evaluate the goodness of fit, robustness and predictive ability. Additionally, the application domain (AD) of the prediction models was characterized with a Williams plot, which is based on standardized residuals (δ^*) and leverage values (h_i).

3. Results and discussion

3.1. log*K* values for organic compounds on graphene and graphene oxides

Experimental log*K* values are available for three of the compounds examined in this study, namely 1,3-dinitrobenzene (DNIN), 4-nitrotoluene (NoT) and nitrobenzene (PhNO2).[14] Table 2 compares our calculated log*K* values with the experimental ones. The mean absolute errors are 0.51 and 0.24 for GS and GO_M, respectively, indicating that molecular dynamics simulation is a viable alternative method for getting log*K* values for adsorption onto graphene nanomaterials.

Table 2. The Experimental and Calculated log*K* Values for DNIN, NoT and PhNO2 on GS and GO_M

Compound	log*K* on GS		log*K* on GO_M	
	Experimental*	Calculated	Experimental*	Calculated
DNIN	5.82	5.76	2.59	3.02
NoT	4.91	5.05	2.79	2.73
PhNO2	5.31	3.99	2.14	1.90

* The experimental log*K* values are obtained from Chen *et al.*'s studies.[14]

Table 1 lists the categories of functional groups for 43 organic compounds and the calculated log*K* values on graphene and graphene oxides. The log*K* values (Fig. 2a) in simulations on unmodified graphene are in the range of 1.70 to 9.65, which is wider than the ranges for each graphene oxides, i.e., 0.93 to 4.06 (GO_H), 1.56 to 6.37 (GO_E), 1.68 to 5.27 (GO_C) and 0.13 to 5.12 (GO_M). The log*K* values for organic compounds on graphene are larger than those on each graphene oxides, namely, GO_H, GO_E and GO_C. Similarly, the lowest free energies for these organic compounds on graphene during the 50-ns simulations are also lower than those on each graphene oxides (Fig. 2b), which implies that graphene has the strongest adsorption capability among these graphene nanomaterials.

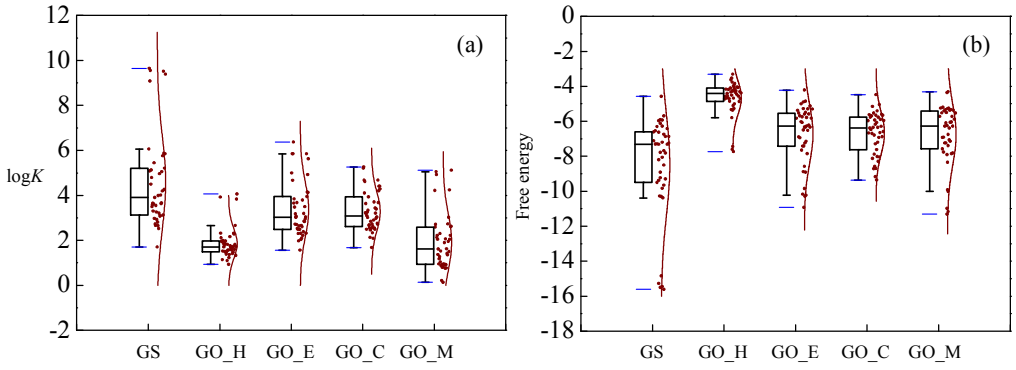

Fig. 2 Whisker and box plot representation of (a) log*K* values and (b) the lowest free energies during the 50-ns simulations on GS, GO_H, GO_E, GO_C and GO_M. The blue lines above and below the rectangles in the plot represent the maximum and minimum log*K* values or free energies on each graphene nanosheet; the top and the bottom of the rectangles represent the 75th and 25th percentiles, respectively; the lines within the rectangles represent 50th percentiles.

3.2. The influence of hydroxyl, epoxy and carbonyl groups for adsorption on graphene oxides

The calculated free energy varies with changing the distance (r) between the center of mass for organic compounds and the surface for graphene and its oxides (Fig. 3 and Fig. S1). Moreover, similar trends were observed in the changes of free energy for 43 compounds on different graphene nanomaterials. In order to explore the effect of hydroxyl, epoxy and carbonyl groups on the adsorption, we focus the discussion on the free energies for the systems including six most representative aromatic compounds, namely, PhH, PhMe, PhOH, PhCN, PhCl and PhNO2 (Fig. 3). For GS, the free energies for organic compounds at the bottom of each valley are −4.58 kcal/mol (PhH), −5.91 kcal/mol (PhMe), −5.93 kcal/mol (PhOH), −7.20 kcal/mol (PhCN), −6.29 kcal/mol (PhCl), and −7.78 kcal/mol (PhNO2). All these values are lower than those on graphene oxides. This further demonstrates that the graphene has the strongest adsorption affinity for these model adsorbates. For GO_H, the free energies for these adsorbates at the bottom of each valley are –3.31 kcal/mol (PhH), −3.53 kcal/mol (PhMe), −3.98 kcal/mol (PhOH), −4.67 kcal/mol (PhCN), −4.28 kcal/mol (PhCl), and −5.12 kcal/mol (PhNO2), and these values are less favorable than those on the other GO models. Thus, graphene oxide with hydroxyl groups has weaker adsorption affinity than the graphene oxides with other functional groups. Note that the bottom of each valley for free energies on GO_H in Fig. 3 locates at ca. 3.8 Å, while it locates at ca. 3.5 Å for the free energies on GS, which may be understood by the fact that steric effects for hydroxyl groups on GO_H hinder the adsorbates from approaching GO_H.

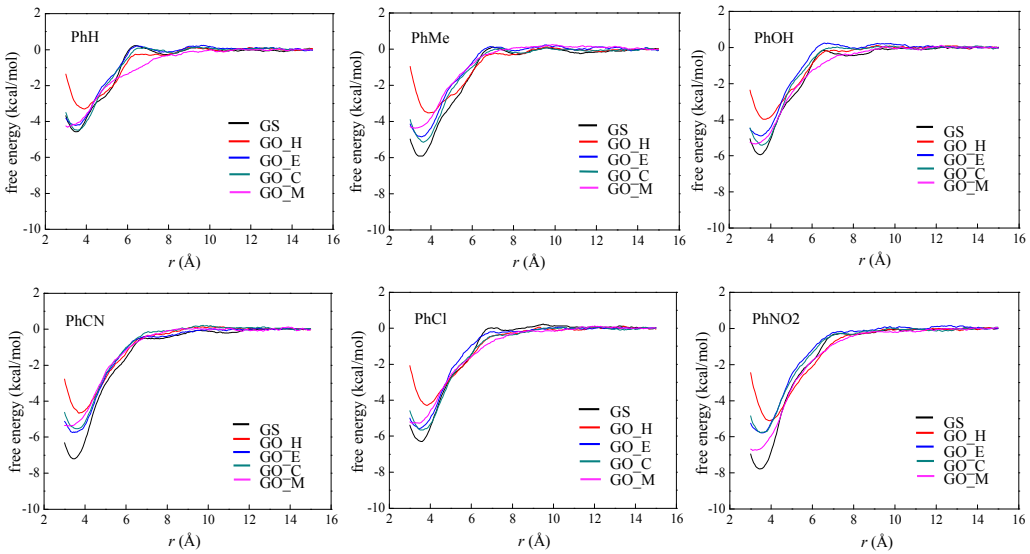

Fig. 3 Calculated free energy versus distance (r) between the center-of-mass for six organic compounds and the surface of graphene or graphene oxide nanosheets.

Furthermore, we calculated radial distribution functions (RDFs) for electron-withdrawing atoms (i.e., N, O, F, Cl, Br, I) in a compound relative to the hydrogen atom in hydroxyl groups on GO_H (Fig. 4). The electron-withdrawing atoms in these compounds, namely chlorobenzene (PhCl), bromobenzene (PhBr), iodobenzene (PhI), phenol (PhOH) and benzonitrile (PhCN), tend to distribute closer to the H atoms on GO_H, as compared to the compound, indicating that there exists electrostatic interactions between these electron-withdrawing atoms and H atoms. Especially for N and O atoms, $g(r)$ has a peak at ca. 2 Å, which is within the range of hydrogen bonding interactions. Thus, electrostatic interactions play important roles in adsorption of organic compounds with electron-withdrawing atoms on GO_H, while for compounds with N or O atoms, hydrogen bonding interactions also contribute to the adsorption onto GO_H.

In addition, we also calculated $g(r)$ for H atoms in the substituent of a compound relative to the O atoms in hydroxyl groups of GO_H. The RDFs (Fig. 4) for toluene

(PhMe), ethylbenzene (PhEt), and propylbenzene (PhPr) indicate that there are no hydrogen bonding interactions between the H atoms of $–CH_3$, $–CH_2CH_3$ and $–CH_2CH_2CH_3$ functional groups and the O atoms of GO_H. The $g(r)$ values for PhOH, 4-fluorophenol (FPl), 3-chlorophenol (ClPl) and phenylmethanol (PhMl), however, have a peak at around 2 Å, implying that hydrogen bonds exist between the hydrogen atom in –OH groups of these four compounds and the O atoms of GO_H. Note that ClPl acts as a hydrogen bond donor and acceptor to –OH group on the GO_H, while 3-bromophenol (BrPl) acts only as a hydrogen bond acceptor. Likewise, m-cresol (mCr) and p-cresol (PCRO) act as hydrogen bond acceptors, though the hydroxyl group in PhOH tends to be a hydrogen bond donor. Therefore, the substituent in a phenol can affect the formation of hydrogen bonds between the –OH and the GO_H. Moreover, RDFs for methylbenzoate (BzOMe) and phenylacetate (PhOAc) in Fig. 4 show that BzOMe has a greater propensity to form hydrogen bonds than PhOAc, even though their structures are similar. The reason may be that the oxygen atom in C=O for BzOMe maintaining the conjugation is richer in electrons than the oxygen atom in C=O for PhOAc, and prefers to act as a hydrogen bond acceptor.

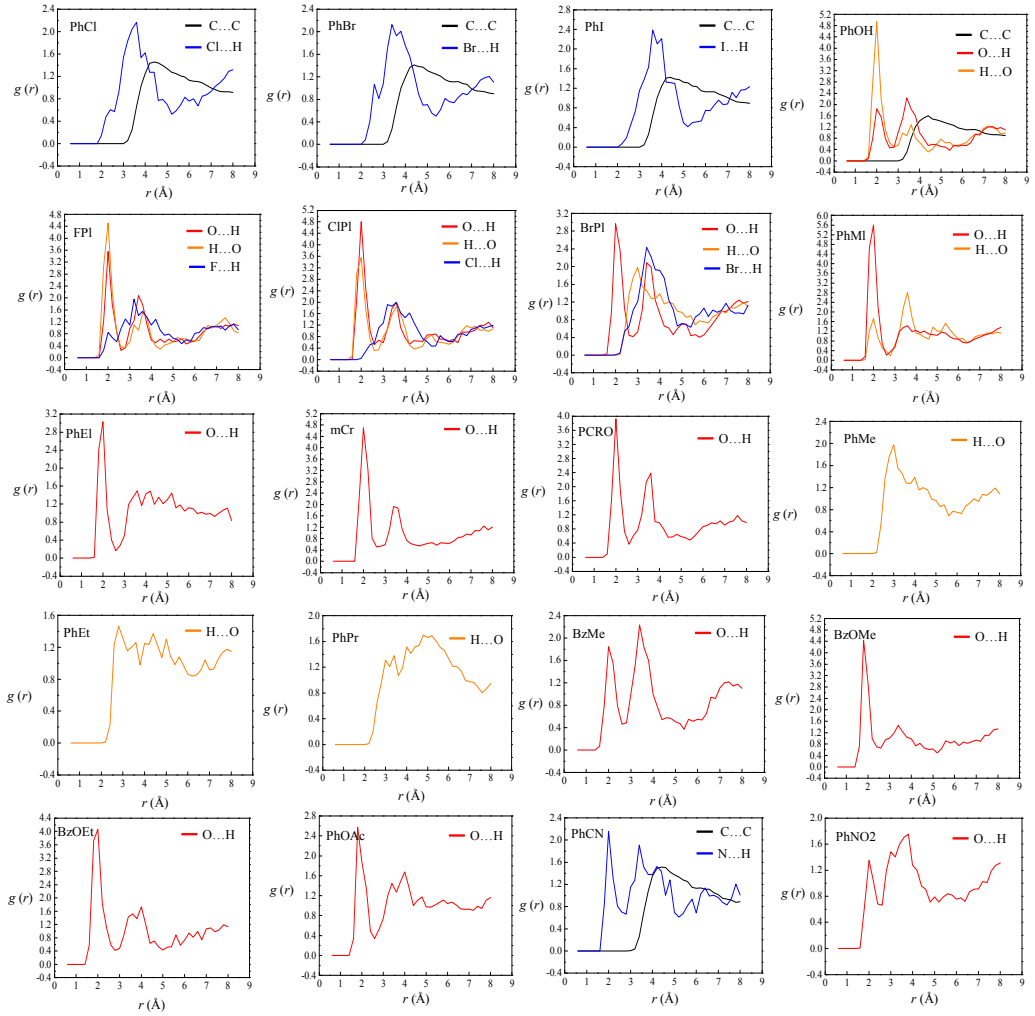

Fig. 4 RDFs for compounds relative to GO_H. C…C: RDFs for all carbon atoms in a compound relative to the graphene nanosheet; H…O: RDFs for H in the substituent of a compound relative to O in the hydroxyl group on GO_H; N…H: RDFs for N in the substituent of a compound relative to H in the hydroxyl group; O…H, F…H, Cl…H, Br…H and I…H were defined similarly.

For graphene oxide with epoxy groups (GO_E), we also examined the RDFs for different atoms, i.e., H atoms in the functional groups –OH, $–CH_3$, $–CH_2CH_3$ and $–CH_2CH_2CH_3$ as well as N atoms in –CN, relative to the O atom in epoxy functional groups (see Fig. S2). None of the RDFs exhibit a peak at ca. 2 Å, indicating that no

hydrogen bonds exist between the inspected organic chemicals and the GO_E nanosheet. Similarly, as for graphene oxide with carbonyl groups (GO_C), the RDFs (Fig. S3) for H atoms in the –OH groups of compounds relative to the O atom on GO_C exhibit a peak at around 2 Å, which reveals that the hydrogen bonding interactions play roles in the adsorption for those compounds having –OH onto GO_C.

As noted above, steric effects result in considerably weaker adsorption for the organic compounds on graphene oxide with hydroxyl groups compared to pristine graphene nanosheets. Graphene oxides with hydroxyl or carbonyl groups can form hydrogen bonds with the –OH group(s) in a compound. The hydroxyl groups in GO_H can also interact with the functional groups, namely, $–CH_2OH$, $–C(O)CH_3$, $–C(O)OCH_3$, $–CH_2CH_2OH$, $–OC(O)CH_3$, $–C(O)OCH_2CH_3$ and –CN via hydrogen bonding. Moreover, the functional group in phenol can affect its hydrogen bonding between its –OH and GO_H.

3.3. Prediction models for adsorption on GS and on GO_M

The optimal models for predicting log$K$ values of organic compounds onto GS and GO_M are as follows.

For GS:

$$\log K = -1.83\varepsilon_\alpha - 1.21\varepsilon_\beta + 1.35q^+ - 1.59q^- + 1.04V - 1.61\pi + 42.06 \quad (3)$$

$n_T = 35$, $R^2 = 0.88$, $RMSE_T = 0.74$, $Q^2_{BOOT} = 0.71$, $n_V = 8$, $Q^2_V = 0.87$, $RMSE_V = 0.54$

For GO_M:

$$\log K = -1.19\varepsilon_\alpha - 0.57\varepsilon_\beta + 5.11q^+ - 1.97q^- + 0.49V + 0.40\pi + 17.77 \quad (4)$$

$n_T = 35$, $R^2 = 0.77$, $RMSE_T = 0.62$, $Q^2_{BOOT} = 0.71$, $n_V = 8$, $Q^2_V = 0.65$, $RMSE_V = 0.53$

where n_T and n_V are the number of compounds in the training set and validation set. Fig. 5(a) shows that the predicted log$K$ values on graphene nanosheets agree well with those determined by MD simulations. Similarly, the predicted log$K$ values on GO_M are in good agreement with those from simulations (Fig. 5(b)). The values for R^2 ($R^2 > 0.60$), Q^2_{BOOT} and Q^2_V ($Q^2 > 0.50$),[58] $RMSE_T$ and $RMSE_V$ indicate that these two models have satisfactory goodness-of-fit, robustness and predictive ability.

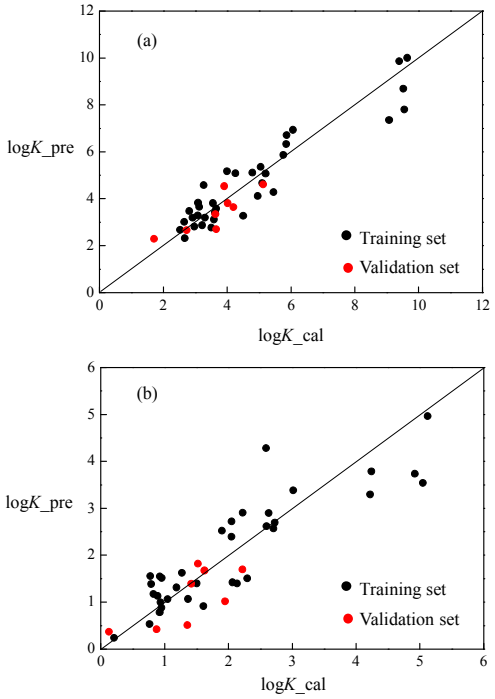

Fig. 5 Predicted log$K$ values (log$K$_pre) versus MD calculated ones (log$K$_cal) on (a) GS and (b) GO_M.

Applicability domains of the prediction models (Eq. 3 and Eq. 4) are visualized in Fig. 6. All the compounds have $|\delta^*| < 3$, which shows that there are no outliers. Eq. 3 can be used for predicting log$K$ values onto graphene nanosheets for various aromatic compounds including benzene, benzyl alcohol, phenol, aniline, nitrobenzene, nitrile,

halogenated benzene, ketone, ester, biphenyl and their derivatives, polycyclic aromatic hydrocarbons (PAHs) and polybrominated diphenyl ethers (PBDEs). Eq. 4, with the same applicability domain as Eq. 3, can predict adsorption onto graphene oxide. Note that these are the first theoretical linear solvation energy relationship models for adsorption onto graphene and graphene oxide.

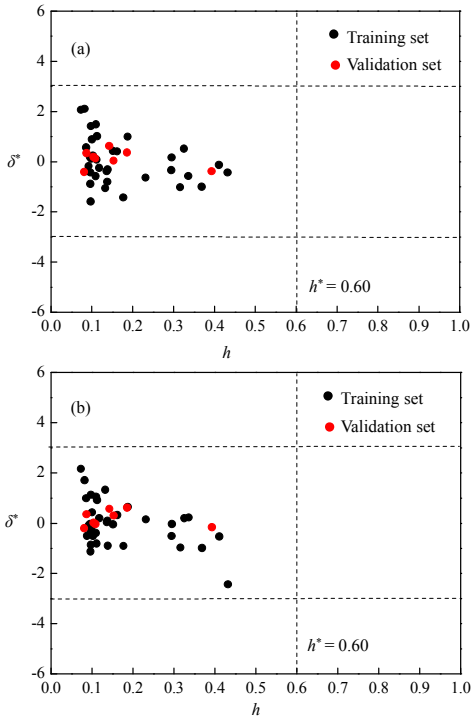

Fig. 6 Williams plot of standardized residuals (δ^*) versus leverages (h) on (a) GS and (b) GO_M.

3.4. Adsorption mechanisms on GS and GO_M

As given in the two prediction models Eq. 3 and Eq. 4, the six terms $a\varepsilon_\alpha$, $b\varepsilon_\beta$, eq^-, fq^+, vV and $p\pi$ have different contributions to the log$K$ values. This difference indicates that hydrogen bonding, dispersion, hydrophobic and electrostatic

interactions play diverse roles in the adsorption of organic compounds onto graphene and graphene oxide.

For adsorption on graphene (Eq. 3), the covalent acidity (ε_α) of the examined organic compounds has a negative contribution to the log$K$ values, indicating that compounds with strong H-donating abilities prefer to form hydrogen bonds with the oxygen atoms in water molecules, leading to a decrease in log$K$. Similarly, the log$K$ values increase with decreasing covalent basicity (ε_β), as compounds with strong H-accepting abilities can interact with the hydrogen atoms in the water molecules as H-acceptors. Electrostatic acidity (q^+) has a positive fitting coefficient, which implies that the increase of q^+ can result in the increase of log$K$ values. It is known that the hydrogen atom with the most positive formal charge can interact with π electrons around graphene, which may promote adsorption of organic compounds onto graphene. On the contrary, the electrostatic basicity (q^-) of a molecule correlates negatively with the log$K$ values.

The term vV, which represents the dispersion and hydrophobic interactions, has a positive contribution to the log$K$ values. In previous prediction models for multiwalled carbon nanotubes,[27, 59] which are based on experimental adsorption data, vV plays an analogous role. Note that the dipolarity/polarizability term ($p\pi$) has a negative fitting coefficient, indicating that compounds possessing larger polarizability tend to interact with water molecules rather than with graphene.

For adsorption onto graphene oxide (Eq. 4), the terms $a\varepsilon_\alpha$, $b\varepsilon_\beta$ and eq^- contribute negatively, while the electrostatic acidity (fq^+) and bulk/cavity (vV) terms are positively correlated with the log$K$ values, similar to those in the graphene prediction model. However, the dipolarity/polarizability ($p\pi$) term makes a positive contribution to the adsorption for organic compounds on graphene oxide, in contrast to graphene.

The reason may be that the hydroxyl and epoxy groups in graphene oxide result in polar surface, which promotes stronger interactions with polarizable compounds. To confirm the above reasoning, we computed the electrostatic potential for graphene and graphene oxide with density functional theory, as detailed in the SI. The electrostatic potential around hydroxyl and epoxy groups are negative (Fig. 7), which differs significantly from that on a graphene nanosheet. This demonstrates that the hydroxyl and epoxy groups on graphene oxide increase the polarity of graphene oxide.

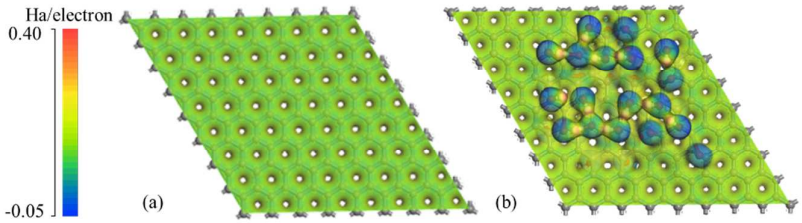

Fig. 7 Electrostatic potential distribution of (a) graphene and (b) GO_M.

Furthermore, we made comparisons among these standardized coefficients for ε_α, ε_β, q^+, q^-, V and π (Table 3). As shown in Table 3, for the graphene prediction model, H-donating ability (ε_α) and dispersion/hydrophobic interactions (V) are the most influential factors on log$K$ values, while for the graphene oxide model, H-donating ability (ε_α) has the most significant effects on log$K$ values.

Table 3. Descriptors and Their standardized coefficients

Descriptors	Standardized coefficients	
	GS	GO_M
ε_α	−0.84	−0.90
ε_β	−0.35	−0.28
q^+	0.06	0.36

q^-	−0.10	−0.21
V	0.46	0.35
π	−0.16	0.07

4. Conclusions

By combining MD simulations and TLSERs, we investigated the adsorption of 43 aromatic solutes on graphene and graphene oxides with the functional groups hydroxyl, epoxy and carbonyl. MD simulations provided us an atomic-level view of the adsorption process and an in-depth understanding of how different functional groups attached to the graphene nanosheet influence adsorption from aqueous solution. The results illustrate that the hydroxyl and carbonyl groups on graphene oxides can form hydrogen bonds with a solute's –OH group, while the epoxy group does not form hydrogen bonds with the same compound. The newly established TLSER models can enable us to obtain the adsorption equilibrium coefficients for a much wider range of uncharged compounds onto graphene nanomaterials than the 43 tested ones in this work. This study provides us promising tools to rapidly predict adsorption affinities onto graphene and graphene oxides using only theoretical molecular structure descriptors, which can overcome the lack of molecular structure descriptors from experimental determination.

Supplementary information

Electronic supplementary information (ESI) is available: (1) 35 compounds in the training set and 8 compounds in the validation set (Table S1); (2) Calculated free energy versus distance (r) between the center-of-mass for 37 organic compounds and the surface of graphene or graphene oxide nanosheets (Fig. S1); (3) Radial

distribution functions on GO_E (Fig. S2); (4) Radial distribution functions on GO_C (Fig. S3); (5) Details for computing the electrostatic potential distribution with density functional theory (DFT) method (SI1).

Corresponding Authors

*James C. Gumbart, Phone: +1-404-385-0797, e-mail: gumbart@physics.gatech.edu.

*Jeffrey Comer, Phone/fax: +1-785-532-6311, e-mail: jeffcomer@ksu.edu.

*Jingwen Chen, Phone/fax: +86-411-84706269, e-mail: jwchen@dlut.edu.cn.

Notes

The authors declare no competing financial interest.

Acknowledgements

The study was supported in USA by NSF (Grant No. HRD-1736093 to ZC; MCB-1452464 to JCG; CHE-1726332 to JC) and NASA (Grant No. 17-EPSCoRProp-0032) and in China by the National Natural Science Foundation of China (21325729, 21661142001). Ya Wang acknowledges a fellowship from the China Scholarship Council. This work used the Extreme Science and Engineering Discovery Environment (XSEDE), which is supported by National Science Foundation grant number ACI-1548562.

References

1 K. S. Novoselov, A. K. Geim, S. V. Morozov, D. Jiang, Y. Zhang, S. V. Dubonos, I. V. Grigorieva and A. A. Firsov, Electric field effect in atomically thin carbon films, *Science*, **2004**, 306, 666−669.

2 Y. Shen, Q. L. Fang and B. L. Chen, Environmental applications of three-dimensional graphene-based macrostructures: Adsorption, transformation, and

detection, *Environ. Sci. Technol*., **2015**, 49, 67−84.

3 M. L. Pan, Y. Y. Zhang, C. Shan, X. L. Zhang, G. D. Gao and B. C. Pan, Flat graphene-enhanced electron transfer involved in redox reactions, *Environ. Sci. Technol*., **2017**, 51, 8597−8605.

4 A. Ambrosi, C. K. Chua, A. Bonanni and M. Pumera, Electrochemistry of graphene and related materials, *Chem. Rev.*, **2014**, 114, 7150−7188.

5 C. Finnerty, L.Zhang, D. L.Sedlak, K. L.Nelson and B. X. Mi, Synthetic graphene oxide leaf for solar desalination with zero liquid discharge, *Environ. Sci. Technol*., **2017**, 51, 11701−11709.

6 S. Navalon, A. Dhakshinamoorthy, M. Alvaro and H. Garcia, Carbocatalysis by graphene-based materials, *Chem. Rev.*, **2014**, 114, 6179−6212.

7 K. S. Novoselov, V. I. Fal'ko, L. Colombo, P. R. Gellert, M. G. Schwab and K. Kim, A roadmap for graphene, *Nature*, **2012**, 490, 192−200.

8 K. P. Loh, Q. L. Bao, G. Eda and M. Chhowalla, Graphene oxide as a chemically tunable platform for optical applications, *Nat. Chem*., **2010**, 2, 1015–1024.

9 A. Zurutuza and C. Marinelli, Challenges and opportunities in graphene commercialization, *Nat. Nanotechnol.*, **2014**, 9, 730−734.

10 Q. Liu, J. B. Shi, J. T. Sun, T. Wang, L. X. Zeng and G. B. Jiang, Graphene and graphene oxide sheets supported on silica as versatile and high-performance adsorbents for solid-phase extraction. *Angew. Chem*. *Int. Ed.*, **2011**, 123, 6035−6039.

11 H. J. Choi, N. A. Kumar and J. B. Baek, Graphene supported non-precious

metal-macrocycle catalysts for oxygen reduction reaction in fuel cells. *Nanoscale*, **2015**, 7, 6991−6998.

12 M. R. Gao, X. Cao, Q. Gao, Y. F. Xu, Y. R. Zheng, J. Jiang and S. H. Yu, Nitrogen-doped graphene supported $CoSe_2$ nanobelt composite catalyst for efficient water oxidation, *ACS Nano*, **2014**, 8, 3970–3978.

13 J. Zhao, Z. Y. Wang, J. C. White and B. S. Xing, Graphene in the aquatic environment: adsorption, dispersion, toxicity and transformation, *Environ. Sci. Technol*., **2014**, 48, 9995−10009.

14 X. X. Chen and B. L. Chen, Macroscopic and spectroscopic investigations of the adsorption of nitroaromatic compounds on graphene oxide, reduced graphene oxide, and graphene nanosheets, *Environ. Sci. Technol*., **2015**, 49, 6181−6189.

15 Z. X. Jin, X. X. Wang, Y. B. Sun, Y. J. Ai and X. K.Wang, Adsorption of 4-n-nonylphenol and bisphenol-A on magnetic reduced graphene oxides: a combined experimental and theoretical studies, *Environ. Sci. Technol*., **2015**, 49, 9168−9175.

16 H. Yan, H. Wu, K. Li, Y. W. Wang, X. Tao, H. Yang, A. M. Li and R. S. Cheng, Influence of the surface structure of graphene oxide on the adsorption of aromatic organic compounds from water, *ACS Appl. Mater. Interfaces*, **2015**, 7, 6690−6697.

17 V. C. Sanchez, A. Jachak, R. H. Hurt and A. B. Kane, Biological interactions of graphene-family nanomaterials: an interdisciplinary review, *Chem. Res. Toxicol.*, **2012**, 25, 15–34.

18 V. Georgakilas, J. N. Tiwari, K. C. Kemp, J. A. Perman, A. B. Bourlinos, K. S.

Kim and R. Zboril, Noncovalent functionalization of graphene and graphene oxide for energy materials, biosensing, catalytic, and biomedical applications, *Chem. Rev.*, **2016**, 116, 5464−5519.

19 A. M. Dimiev, L. B. Alemany and J. M. Tour, Graphene oxide. origin of acidity, its instability in water, and a new dynamic structural model, *Acs Nano*, **2013**, 7, 576−588.

20 H. Tang, Y. Zhao, X. N. Yang, D. M. Liu, P. H. Shao, Z. G. Zhu, S. J. Shan, F. Y. Cui and B. S. Xing, New insight into the aggregation of graphene oxide using molecular dynamics simulations and extended Derjaguin–Landau–Verwey–Overbeek theory, *Environ. Sci. Technol*., **2017**, 51, 9674–9682.

21 S. Osella, A. Minoia and D. Beljonne, Combined molecular dynamics and density functional theory study of azobenzene–graphene interfaces, *J. Phys. Chem. C*., **2016**, 120, 6651–6658.

22 A. Rissanou and V. Harmandaris, Structure and dynamics of poly(methyl methacrylate)/graphene systems through atomistic molecular dynamics simulations, *J. Nanopart. Res*., **2013**, 15, 1589.

23 L. Y. Xu and X. N. Yang, Molecular dynamics simulation of adsorption of pyrene–polyethylene glycol onto graphene, *J. Colloid. Interf. Sci.*, **2014**, 418, 66–73.

24 Y. Wang, J. W. Chen, X. X. Wei, A. J. Hernandez-Maldonado and Z. F. Chen, Unveiling adsorption mechanisms of organic pollutants onto carbon nanomaterials by DFT computations and pp-LFER modeling, *Environ. Sci. Technol*., **2017**, 51,

11820−11828.

25 G. R. Famini and L. Y. Wilson, Using theoretical descriptors in linear free energy relationships: characterizing several polarity, acid and basicity scales, *J. Phys. Org. Chem.*, **1999**, 12, 645–653.

26 G. R. Famini and L. Y. Wilson, Using theoretical descriptors in quantitative structure activity relationships: application to partition properties of alkyl (1-phenylsulfonyl) cycloalkane-carboxylates, *Chemosphere*, **1997**, 35, 2417–2447.

27 X. R. Xia, N. A. Monteiro-Riviere and J. E. Riviere, An index for characterization of nanomaterials in biological systems, *Nat. Nanotech*., **2010**, 5, 671−675.

28 J. Comer, R. Chen, H. Poblete, A. Vergara-Jaque and J. E. Riviere, Predicting adsorption affinities of small molecules on carbon nanotubes using molecular dynamics simulation, *ACS. Nano*, **2015**, 9, 11761−11774.

29 R. Chen, Y. T. Zhang, N. A. Monteiro-Riviere and J. E. Riviere, Quantification of nanoparticle pesticide adsorption: computational approaches based on experimental data, *Nanotoxicology*, **2016**, 10, 1118−1128.

30 S. Agnihotri, M. J. Rood and M. Rostam-Abadi, Adsorption equilibrium of organic vapors on single-walled carbon nanotubes, *Carbon*, **2005**, 43, 2379−2388.

31 A. K. Chopra, M. K. Sharma and S. Chamoli, Bioaccumulation of organochlorine pesticides in aquatic system—an overview, *Environ. Monit. Assess.*, **2011**, 173, 905−916.

32 M. Iqbal, J. H. Syed, A. Katsoyiannis, R. N. Malik, A. Farooqi, A. Butt, J. Li, G.

Zhang, A. Cincinelli and K. C. Jones, Legacy and emerging flame retardants (FRs) in the freshwater ecosystem: A review, *Environ. Res.*, **2017**, 152, 26−42.

33 A. Baumer, K. Bittermann, N. Klüver and B. I. Escher, Baseline toxicity and ion-trapping models to describe the pH-dependence of bacterial toxicity of pharmaceuticals, *Environ. Sci.: Processes Impacts*, 2017, **19**, 901–916.

34 B. I. Escher and R. P. Schwarzenbach, Mechanistic studies on baseline toxicity and uncoupling of organic compounds as a basis for modeling effective membrane concentrations in aquatic organisms, *Aquat. Sci.*, **2002**, 64, 20–35.

35 Royal Society of Chemistry. *ChemSpider*; **2017**; http://www.chemspider.com.

36 *ChemicalBook*; 2017; https://www.chemicalbook.com/

37 K. Vanommeslaeghe, E. Hatcher, C. Acharya, S. Kundu, S. Zhong, J. Shim, E. Darian, O. Guvench, P. Lopes, I. Vorobyov and A. D. Mackerell, Jr., CHARMM general force field: A force field for drug-like molecules compatible with the CHARMM all-atom additive biological force fields, *J. Comput. Chem*., **2010**, 31, 671–690.

38 K. Vanommeslaeghe and A. D. MacKerell, Jr., Automation of the CHARMM General Force Field (CGenFF) I: Bond perception and atom typing, *J. Chem. Inf. Model.*, **2012**, 52, 3144–3154.

39 K. Vanommeslaeghe, E. P. Raman and A. D. MacKerell, Jr., Automation of the CHARMM General Force Field (CGenFF) II: Assignment of bonded parameters and partial atomic charges, *J. Chem. Inf. Model.*, **2012**, 52, 3155–3168.

40 T. P. Senftle, S. Hong, M. M. Islam, S. B. Kylasa, Y. X. Zheng, Y. K. Shin, C.

Junkermeier, R. Engel-Herbert, M. J. Janik, H. M. Aktulga, T. Verstraelen, A. Grama and A. C. T. van Duin, The ReaxFF reactive force-field: development, applications and future directions, *npj. Comp. Mater.*, **2016**, 2, 15011.

41 H. M. Aktulga, J. C. Fogarty, S. A. Pandit and A. Y. Grama, Parallel reactive molecular dynamics: Numerical methods and algorithmic techniques, *Parallel. Computing.*, **2012**, 38, 245–259.

42 S. Plimpton. Fast parallel algorithms for short-range molecular dynamics, *J. Comput. Phys.*, **1995**, 117, 1–19.

43 J. C. Phillips, R. Braun, W. Wang, J. Gumbart, E. Tajkhorshid, E. Villa, C. Chipot, R. D. Skeel, L. Kale and K. Schulten, Scalable Molecular Dynamics with NAMD, *J. Comput. Chem.*, **2005**, 26, 1781–1802.

44 X. R. Xia, N. A. Monteiro-Riviere, S. Mathur, X. Song, L. Xiao, S. J. Oldenberg, B. Fadeel and J. E. Riviere, Mapping the Surface Adsorption Forces of Nanomaterials in Biological Systems, *ACS Nano*, **2011**, 5, 9074–9081.

45 W. L. Jorgensen, J. Chandrasekhar, J. D. Madura, R. W. Impey and M. L. Klein, Comparison of simple potential functions for simulating liquid water, *J. Chem. Phys.*, **1983**, 79, 926−935.

46 S. E. Feller, Y. H. Zhang, R. W. Pastor and B. R. Brooks, Constant pressure molecular dynamics simulations: The Langevin piston method, *J. Chem. Phys.*, **1995**, 103, 4613–4621.

47 U. Essmann, L. Perera, M. L. Berkowitz, T. Darden, H. Lee and L. G. Pedersen, A

smooth particle mesh Ewald method, *J. Chem. Phys*., **1995**, 103, 8577−8593.

48 W. Humphrey, A. Dalke and K. Schulten, VMD – Visual molecular dynamics, *J. Mol. Graphics*, **1996**, 14, 33–38.

49 E. Darve and A. Pohorille, Calculating free energies using average force, *J. Chem. Phys.*, **2001**, 115, 9169−9183.

50 J. Comer, J. C. Gumbart, J. Hénin, T. Lelièvre, A. Pohorille and C. Chipot, The adaptive biasing force method: everything you always wanted to know, but were afraid to ask. *J. Phys. Chem.*, *B* **2015**, 119, 1129−1151.

51 G. Fiorin, M. L. Klein and J. Hénin, Using collective variables to drive molecular dynamics simulations, *Mol. Phys.*, **2013**, 111, 3345–3362.

52 Y. Zhao and D. Truhlar, The M06 suite of density functionals for main group thermochemistry, thermochemical kinetics, noncovalent interactions, excited states, and transition elements: two new functionals and systematic testing of four M06-class functionals and 12 other functionals, *Theor. Chem. Acc*., **2008**, 120, 215−241.

53 M. J. Frisch, G. W. Trucks, H. B. Schlegel, G. E. Scuseria, M. A. Robb, J. R. Cheeseman, G. Scalmani, V. Barone, B. Mennucci, G. A. Petersson, H. Nakatsuji, M. Caricato, X. Li, H. P. Hratchian, A. F. Izmaylov, J. Bloino, G. Zheng, J. L. Sonnenberg, M. Hada, M. Ehara, K. Toyota, R. Fukuda, J. Hasegawa, M. Ishida, T. Nakajima, Y. Honda, O. Kitao, H. Nakai, T. Vreven, J. A. Montgomery, Jr. J. E. Peralta, F. Ogliaro, M. Bearpark, J. J. Heyd, E. Brothers, K. N. Kudin, V. N. Staroverov, R. Kobayashi, J. Normand, K. Raghavachari, A. Rendell, J. C. Burant, S.

S. Iyengar, J. Tomasi, M. Cossi, N. Rega, J. M. Millam, M. Klene, J. E. Knox, J. B. Cross, V. Bakken, C. Adamo, J. Jaramillo, R. Gomperts, R. E. Stratmann, O. Yazyev, A. J. Austin, R. Cammi, C. Pomelli, J. W. Ochterski, R. L. Martin, K. Morokuma, V. G. Zakrzewski, G. A. Voth, P. Salvador, J. J. Dannenberg, S. Dapprich, A. D. Daniels, O. Farkas, J. B. Foresman, J. V. Ortiz, J. Cioslowski and D. J. Fox, Gaussian 09, Revision A. 01; Gaussian, Inc.: Wallingford CT, **2009**.

54 W. R. Wadt and P. J. Hay, Ab initio effective core potentials for molecular calculations. Potentials for main group elements Na to Bi, *J. Chem. Phys*., **1985**, 82, 284−298.

55 Talete srl, 2012. Dragon (Software for Molecular Descriptor Calculation) Version 6.0. http://www.talete.mi.it/.

56 J. S. Murray, P. Politzer and G. R. Famini, Theoretical alternatives to linear solvation energy relationships, *J. Mol. Struct.-Theochem*, **1998**, 454, 299−306.

57 L. Y. Wilson and G. R. Famini, Using theoretical descriptors in quantitative structure-activity relationships: some toxicological indices, *J. Med. Chem*., **1991**, 34, 1668-1674.

58 A. Golbraikh, M. Shen, Z. Y. Xiao, Y. D. Xiao, K. H. Lee and A. Tropsha, Rational selection of training and test sets for the development of validated QSAR models, *J. Comput. Aided. Mol. Des.*, **2003**, 17, 241−253.

59 O. G. Apul, Q. L. Wang, T. Shao, J. R. Rieck and T. Karanfil, Predictive model development for adsorption of aromatic contaminants by multi-walled carbon

nanotubes, *Environ. Sci. Technol.*, **2013**, 47, 2295−2303.

Exploring adsorption of neutral aromatic pollutants onto graphene nanomaterials via molecular dynamics simulations and theoretical linear solvation energy relationships

Ya Wang,[abc] Jeffrey Comer,[*d] Zhongfang Chen,[c] Jingwen Chen,[*b] James C. Gumbart[*a]

[a] School of Physics, Georgia Institute of Technology, Atlanta, GA 30332, USA

[b] Key Laboratory of Industrial Ecology and Environmental Engineering (MOE), School of Environmental Science and Technology, Dalian University of Technology, Linggong Road 2, Dalian 116024, China

[c] Department of Chemistry, University of Puerto Rico, San Juan, PR 00931, USA

[d] Institute of Computational Comparative Medicine, Nanotechnology Innovation Center of Kansas State, Department of Anatomy and Physiology, Kansas State University, Manhattan, Kansas 66506-5802, USA

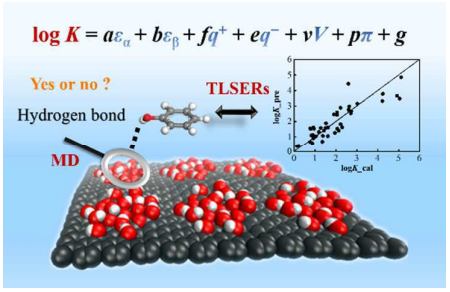

TLSER models were developed for the first time to predict the adsorption equilibrium coefficients onto graphene and graphene oxide nanosheets.